ELSEVIER

Biochimica et Biophysica Acta 1281 (1996) 5–14

BBA Biochimica et Biophysica Acta

Forces on biological cells due to applied alternating (AC) electric fields. II. Electro-rotation

Tohsak L. Mahaworasilpa *, Hans G.L. Coster, Eric P. George

UNESCO Centre for Membrane Science and Technology, Department of Biophysics, School of Physics, University of New South Wales, P.O. Box 1, Kensington, N.S.W. 2033, Australia

Received 7 June 1995; revised 26 October 1995; accepted 9 November 1995

Abstract

Measurements are presented of angular velocities of rotation of mammalian cells of K562 (human) and SP2 (mouse) in external alternating electric fields over a frequency range of 0.5 kHz to 12 MHz. Electro-rotation of the cells was observed for the case of 'two cells in contact' using two parallel, cylindrical electrodes; only one cell was located on the electrode. A theoretical analysis is also presented which shows that the cell rotation arises from a torque produced by the interaction between the *primary electric dipole moment* induced in the spinning cell and the secondary electric fields, generated by the primary dipole induced in the adjacent cell. These secondary fields are out of phase with the applied electric field. The results show that (a) only the cell not located on the electrode rotates, (b) maximal electro-rotation occurs at *two different excitation field frequency domains* for the frequency range employed here, (c) the spin speed of the rotating cell at each frequency domain is much less than the excitation frequency, (d) the rotation direction of the cell depends on the angle (θ) between the external electric field and the line joining the centres of the two cells and (e) for a given angle θ, the rotation direction is the same for both excitation frequency domains. The experimental measurements allowed us to estimate the conductivities of the cytoplasms and membrane capacitances of the cells of K562 and SP2. The conductivities of the cytoplasms of the cells of K562 and SP2 were estimated to be 0.2 and 0.3 $S\,m^{-1}$, respectively, whereas the membrane capacitances of these cells were found to be 2.7 ± 0.8 and 9.8 ± 0.6 $mF\,m^{-2}$, respectively.

Keywords: Electrorotation; Cell electrodynamics; Induced electric dipole; Cell membrane; Membrane capacitance

1. Introduction

Electro-rotation provides a potentially useful tool for the study of the electrical properties of biological cells. It is a non-invasive technique which allows (a) separation of viable from non-viable biological cells [1] or (b) to make comparison of the electrical properties of the same types or different kinds of cells (such as T and B lymphocytes) but at various immunological, pathogenic stages or chemical stimulations [2–5]. When very small particles such as biological cells are in an electric field, electro-rotation of these particles may be observed either in an alternating electric field using a two-electrode technique [6,7,23] or in a rotating electric field using three or four electrodes with two external electric fields which are out of phase to each other [9,10,13,14].

Early experiments on the rotation of biological cells in alternating electric fields were carried out using a simple two-electrode system [6,11]. While a number of experiments and studies have appeared in the literature, few theoretical analyses have been reported (e.g. [12,24]). For the analysis of the experimental results, Arnold and Zimmermann [9] adopted a single spherical dielectric shell model for the cell and employed an external rotating electric field to investigate the rotation of a mesophyll protoplast. They reported that there were only two characteristic rotating frequencies. Fuhr and Kuzmin [10] employed a two-layer model consisting of two spherical shells and three dielectrics as a model of the cell for their analysis of the electro-rotation of a single plant cell (using

* Corresponding author. Fax: +61 2 3855981; e-mail: tohsak@unsw.edu.au.

SSDI 0005-2736(95)00271-5

rotating electric fields). The first dielectric represented the cytoplasm, the second dielectric and the first shell represented the plasma membrane whilst the third dielectric and the second shell represented the cell wall. With the two-layer model proposed, they suggested that the system should have three characteristic rotating frequencies. Arnold et al. [15] observed rotation of mouse oocytes at two different field frequency ranges, i.e. 1 to 100 kHz and 0.2 to 2 MHz with maximum spin speeds at 5 kHz and 1 MHz, respectively. In the low-frequency domain, the cells rotated in the opposite direction to the direction of the rotating electric field (anti-field), whereas in the high-frequency region, the cells rotated in the same direction to the rotating field (co-field).

Although cell rotation obtained by using an external rotating electric field has been used as a tool for estimating the electrical properties of cell membranes, a two-electrode technique is simpler and requires only a single simple AC signal generator. The cell rotation in this case occurs when two cells are in close proximity whereupon the induced dipoles establish a local rotating field.

This work reports the experimental results from the electro-rotation of two mammalian cell lines (K562 and SP2 cell lines) in an applied AC field using two parallel wire electrodes, over a frequency range of 0.5 kHz to 12 MHz, in a hypotonic sorbitol solution (100 mM). A theoretical analysis of the rotation in terms of the induced dipole moments of the adjacent cells is also presented.

2. Materials and methods

K562 and SP2 cells were obtained from their own cultures which had been passaged with RPMI + 10% FCS medium at regular intervals. Details of cell preparation have been described previously [8]. Measurements of cell rotation angular velocity were made in 100 mM sorbitol using (a) a cell chamber, (b) two uncoated nickle alloy, parallel wires (128 μm in diameter), (c) an alternating (AC) electric signal generator with variable amplitude and frequency, and (d) an optical/video-recording system as described previously [8].

For each measurement, two washed cells were deposited on one of the parallel electrodes. The two electrodes were 300 μm apart throughout the experiments. The electrode and cell configuration is shown in Fig. 1. By applying an AC potential difference V_t across the parallel electrodes, an external alternating electric field E_o was produced (i.e. $E_o = E_m \cos \omega t$). The amplitude and frequency of the applied AC potential across the electrodes was monitored on an oscilloscope. Due to the geometry of the electrodes, the electric field in the space between the electrodes is *not uniform* but varies with position (z) between the electrodes; the value is readily calculated from the known geometry (see [8]). In the present study, the cell orientation, θ, was defined as the angle between the external field direction, $\mathbf{E}_o$, and the line joining the centres of the two cells, $\mathbf{r}$. θ was assigned to be *positive* in the *clockwise* direction with respect to $\mathbf{E}_o$ (Fig. 1).

3. Data collection and analysis

In the present study, we define the 'spin resonant frequency' (SRF) as the applied electric field frequency at which the 'maximum spin speed' of the rotating cell occurs, whereas the 'excitation field frequency' (EFF) of a rotating cell is simply the applied electric field frequency.

The rotation of K562 and SP2 cells suspended in 100 mM sorbitol solution was evaluated over the frequency range of 0.5 kHz to 12 MHz and for electric field strengths (E_o) of 10, 15, 17.5 and 20 kV m^{-1}.

The behaviour of the cells in the electric field for each cell type and for a given field strength was recorded on a video tape. Video re-plays of the rotation of the cell on a frame by frame basis allowed the spin speed of the cell to be measured with high accuracy. For each excitation field frequency, the spin speed (Ω) as well as the direction of the cell rotation was determined by measuring the times required for 1, 5 and 10 revolutions of the rotating cell. The mean of the time, t, required for one revolution was then evaluated to yield Ω. For a particular excitation field frequency, the process above was repeated for a number of cells of a given cell line.

4. Theoretical analysis

The general solution for the electric field and induced dipole moment at the centre of each cell of the two cells (cell A and B – see Fig. 1), and the torque on cell A is given in Appendix A . For the case where only two cells are in contact and subject to an external, uniform alternating electric field $\mathbf{E}_o$ (Fig. 13), the torque (τ) on the rotating cell is given by (see Eq. A-34 in Appendix A)

$$\overline{\tau}_t = 3\pi\varepsilon_s R^3 E_m'^2 \sin 2\theta \left(\frac{\mathrm{Im}^2[f(\omega)]}{4 - \mathrm{Re}[f(\omega)]} \right) \quad (1)$$

where $\overline{\tau}_t$ is the time-averaged torque, $\mathrm{Re}[f(\omega)]$ and $\mathrm{Im}[f(\omega)]$ are the real and imaginary parts of $f(\omega)$, which are given by Eq. A-35 and Eq. A-36.

Since the external electric field employed in the present study was non-uniform (i.e. $E_m = E_m(z)$), the actual field strength $\mathbf{E}_A$ at the centre of the rotating cell (cell A) must be determined. For parallel electrodes used here, E_A can be calculated from the analysis presented by Mahaworasilpa et al. [8].

At equilibrium, the angular velocity ($\boldsymbol{\Omega}$) of the rotating cell A can be obtained by the balance between the torque and viscous drag ($\mathbf{F}_f$) which is given by $\mathbf{F}_f = -8\pi\eta R^3 \boldsymbol{\Omega}$;

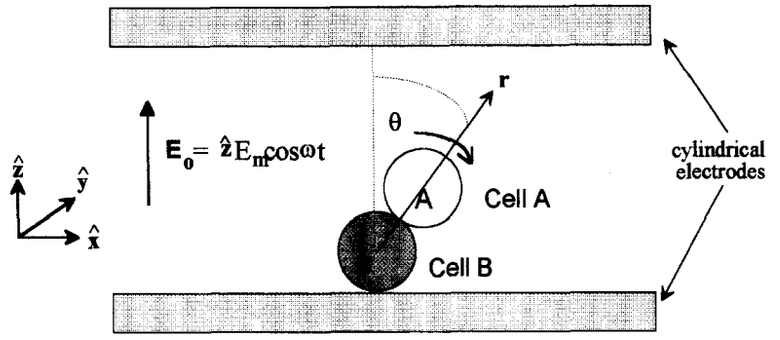

Fig. 1. A two cell configuration used for the present study (not to scale).

where η is the viscosity of the suspending medium [22]. That is

$$\Omega = \frac{3\varepsilon_s}{8\eta} E_m^2 \sin 2\theta \left(\frac{\mathrm{Im}^2[f(\omega)]}{4 - \mathrm{Re}[f(\omega)]} \right) \quad (2)$$

5. Results

5.1. For K562 cells

It was observed that electro-rotation of K562 cells occurred only for cell A, that is, the cell which was not located on the electrode (Fig. 1). Fig. 2 shows that there were two excitation field frequency regions where the cells were observed to spin; that is, between 3 to 20 kHz (with SRF at 15 kHz)) and another region greater than 2.9 MHz. The signal generator used was limited to 12 MHz and hence excitation field frequencies beyond this limit could not be investigated. The cell was observed to spin about an axis perpendicular to the plane constituted by $\mathbf{E}_0$ and $\mathbf{r}$ (see Fig. 1). The cells rotated in the same direction throughout the frequency range investigated. At frequencies below 3 kHz the cells were adversely effected and lysed by the applied field.

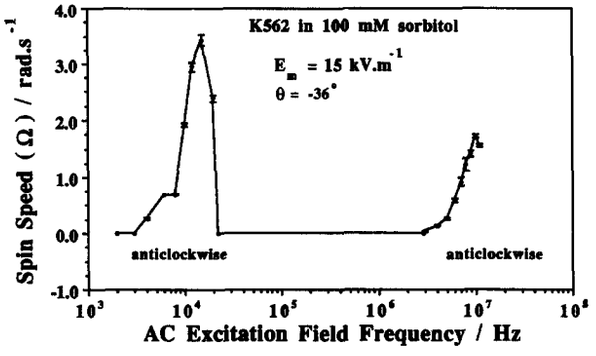

Fig. 2. An experimental plot of spin speed against AC excitation field frequency for K562 cells. Note that the spinning cell rotated anticlockwise for both frequency domains for the nagative value of θ.

Fig. 3 shows that in the *low-frequency region* and for a given external electric field strength, the spin speed of the rotating cell at $\theta = -36°$ is higher than that at $\theta = -23°$. For a given excitation field frequency and a given external electric field strength the rotating cell rotated with the maximum speed at $\theta = -45°$ (Table 1). It was found that for a given orientation of the two cells in the electric field

Table 1
A summary of spin speeds of K562 cells for two different cell orientations (θ) and three different electric field strengths

Electric field intensity (kV m^{-1})	Cell spin speed (rad s^{-1})	
	$\lvert\theta\rvert = 36°$	$\lvert\theta\rvert = 45°$
20	1.2±0.1	2.0±0.1
30	3.0±0.1	4.2±0.1
35	4.4±0.1	5.7±0.1

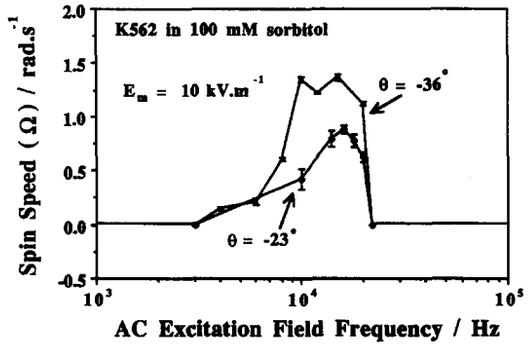

Fig. 3. Experimental plots of spin speed against AC excitation field frequency in the low-frequency domain for K562 cells for two different cell orientations (θ).

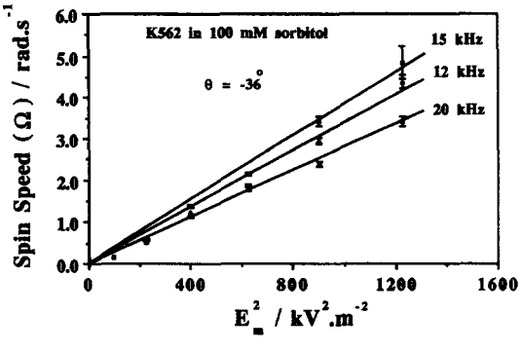

Fig. 4. A family (experimental) plot of spin speed of K562 cells as a function of the square of the field strength for the three different field frequencies; i.e. 12, 15 and 20 kHz.

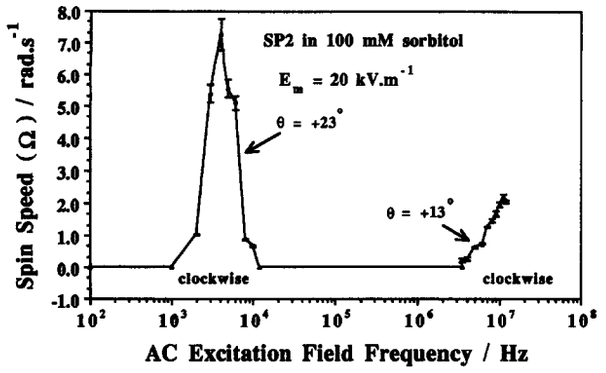

Fig. 5. An experimental plot of spin speed against AC excitation field frequency for SP2 cells. Note that the spinning cell rotated clockwise in both frequency regions for the positive values of θ.

(e.g. $\theta = -36°$), the spin speed (Ω) of the rotating cell in the *low-frequency region* varied as E_m^2 (Fig. 4). Similar results have been reported elsewhere [12].

5.2. For SP2 cells

SP2 cells were observed to spin in a similar manner to those of K562 cells. Two excitation field frequency regions were found; between 1 kHz and 11 kHz for the low-frequency region with SRF of approximately 4 kHz and at excitation frequencies greater than ≈ 3.5 MHz for the high frequency region (Fig. 5). Note that the spin velocities Ω of SP2 cells indicated in the figure were taken at different angles θ, $+23°$ and $+13°$, for the low- and high-frequency regions, respectively. As with K562 cells, the spin speed of the cell, for a given cell orientation (θ), varied as E_m^2.

6. Discussion

The results obtained from the present study showed that for a given cell type, e.g. K562, and a given cell orientation, the rotating cell rotated in the *same direction* over the entire range of the external electric field frequency employed (Figs. 2 and 5). The rotation direction of the rotating cell was observed to be dependent upon the orientation (θ) of the cell. When θ was negative (Fig. 2), the cell was observed to spin *anticlockwise* throughout the range of field frequency investigated. The observations from the present study agreed well with the theoretical analysis presented.

The single direction of cell rotation reported in the present work was in contrast to that reported by other investigators [2,10,15] who found that the direction of cell rotation in the low-frequency region (anti-field) was in the opposite direction to that observed in the high-frequency region (co-field). The results are not contradictory since in these studies the investigators used rotating applied electric fields (established using four electrodes and out-of-phase signal generators). In the present experiments the rotating field is established by the induced dipoles of the adjacent cells; the dipole field being out of phase with the applied unidirectional AC field.

6.1. Effects of specific membrane capacitance (C_m)

Fig. 6 shows theoretical plots of the cell spin speed (Ω) calculated from Eq. (2) as a function of the electric field frequency for various specific membrane capacitances, C_m. It indicates that for the low excitation field frequency (EFF) region (i.e. $< 10^5$ Hz), the spin resonant frequency (SRF) is shifted towards lower excitation field frequencies as the specific membrane capacitance increases, whereas for the high excitation field frequency region (i.e. $> 3 \cdot 10^6$ Hz) the spin resonant frequency is independent of the membrane capacitance. It also shows that the maximum spin speed, Ω, increases slightly as the specific membrane capacitance increases for both field frequency regions. The theoretical plots suggest that the spectral shift in the spin resonant frequency in the low field frequency region is associated with the electrical properties of the cell membrane and that the specific membrane capacitance, C_m, may be estimated from the spin resonant frequency in the low field frequency region [4]. Also the details of the spectra might allow us to classify the type of cell being investigated.

6.2. Effects of the conductivity of the extracellular medium (σ_s)

It was found from the theoretical plots in Fig. 7 that the conductivity of the extracellular fluid, σ_s, is responsible for a shift in the SRF of the cell in the low-frequency region only; for a given conductivity of the cell cytoplasm (σ_c), the SRF is shifted toward higher field frequencies as the conductivity of the external medium, σ_s, is increased. A similar result has been reported elsewhere [15,16].

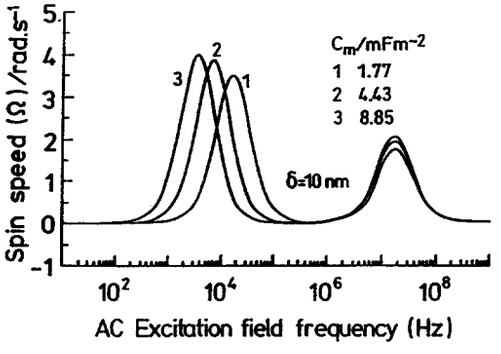

Fig. 6. A family (theoretical) plot of cell spin speed versus AC excitation field frequency for various specific membrane capacitances (C_m). The following parameters were used for these plots: $\varepsilon_s = 80\varepsilon_o$, $\varepsilon_c = 60\varepsilon_o$, $\sigma_s = 1$ mS m^{-1}, $\sigma_c = 0.2$ S m^{-1}, $\sigma_m = 10^{-7}$ S m^{-1}, $R = 10$ μm, $\delta = 10$ nm, $\eta = 1.05$ mN s m^{-2}, $\theta = -36°$.

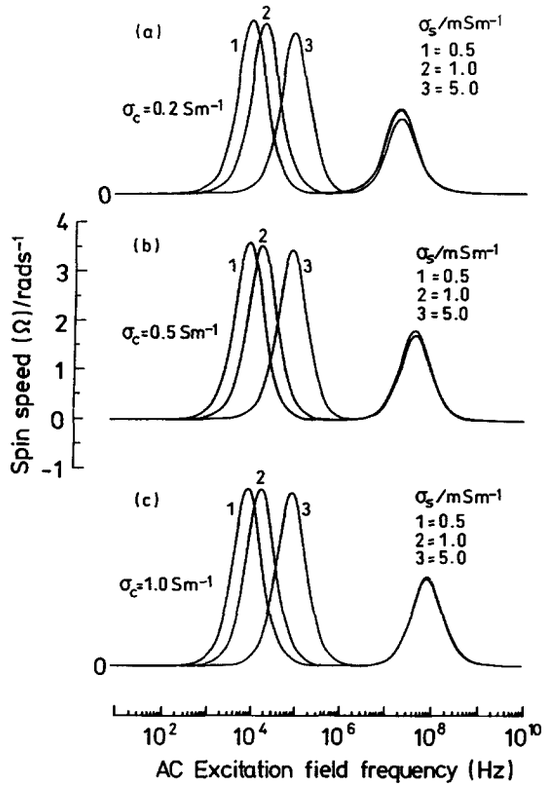

Fig. 7. Effects of the conductivity of the external medium, σ_s, on the spin resonant frequency. The following parameters were used for these theoretical plots: $E'_m = 12$ kV m^{-1}, $\varepsilon'_s = 80\varepsilon_o$, $\varepsilon_c = 60\varepsilon_o$, $\varepsilon_m = 3\varepsilon_o$, $\sigma_m = 10^{-7}$ S m^{-1}, $R = 10$ μm, $\delta = 10$ nm, $\eta = 1.05$ mN s m^{-2}, $\theta = -36°$.

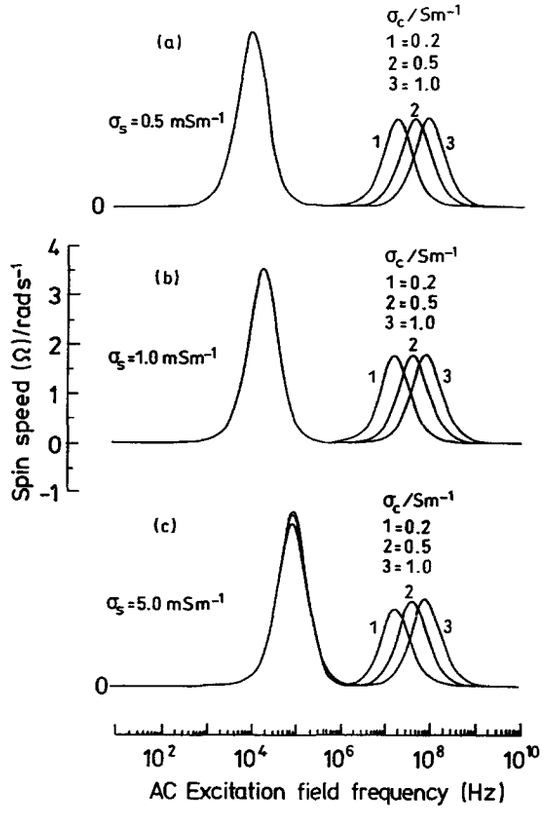

Fig. 8. Effects of the conductivity of the cell cytoplasm, σ_c, on the spin resonant frequency. The following parameters were used for these theoretical plots: $E'_m = 12$ kV m^{-1}, $\varepsilon_s = 80\varepsilon_o$, $\varepsilon_c = 60\varepsilon_o$, $\varepsilon_m = 3\varepsilon_o$, $\sigma_m = 10^{-7}$ S m^{-1}, $R = 10$ μm, $\delta = 10$ nm, $\eta = 1.05$ mN s m^{-2}, $\theta = -36°$.

6.3. Effects of the conductivity of the cell cytoplasm (σ_c)

In the high frequency region, the SRF of the cell is strongly affected by σ_c. Fig. 8 shows theoretically that for a given conductivity of the extracellular medium (σ_s), the SRF is shifted towards higher excitation field frequencies and the amplitude of the maximum spin speed slightly increases when σ_c increases. The variation of σ_c does not affect the SRF in the low frequency region.

6.4. Experimental and theoretical fitting

The theoretically predicted peak in the spin speed in the low frequency excitation region is dependent on the specific membrane capacitance (Fig. 6). Experimental data on spin speed can therefore be used to evaluate the specific capacitance of the cell membrane. Figs. 9 and 10 show the experimental and the theoretical predicted spin speeds (Ω) against excitation field frequency for K562 and SP2 cells for cell orientations $\theta = -36°$ and $+23°$, respectively. The experimental data for K562 and SP2 cells were obtained in experiments using applied electric field strengths of 15 and 20 kV m^{-1}, respectively. To match the peak values of the spin speed, it was necessary to set the field strength in Eq. (2) to 12 and 18 kV m^{-1} for K562 and SP2 cell data, respectively. It will be noted that the detailed form of the experimental and theoretical plots do not coincide precisely. The peak spin frequency is readily accommodated but the peak spin speed was lower than that predicted for a given field strength. This could result from:

(1) The friction between spinning cell (cell A) and the stationary cell (cell B) when the spinning cell was rotating.

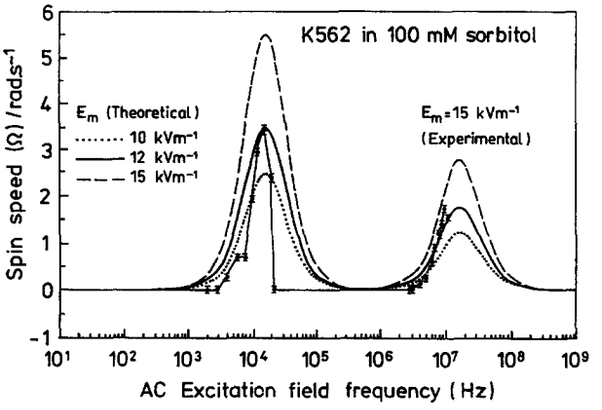

Fig. 9. A fitting between the experimental and theoretical spin speeds for K562 cells for the various values of the external electric field strengths (i.e. 10, 12 and 15 kV m^{-1}). The following parameters were used for these theoretical plots: $\varepsilon_s = 80\varepsilon_o$, $\varepsilon_c = 60\varepsilon_o$, $\varepsilon_m = 3\varepsilon_o$, $\sigma_s = 1$ mS m^{-1}, $\sigma_c = 0.2$ S m^{-1}, $\sigma_m = 10^{-7}$ S m^{-1}, $R = 10$ μm, $\delta = 10$ nm, $\eta = 1.05$ mN s m^{-2}, $\theta = -36°$.

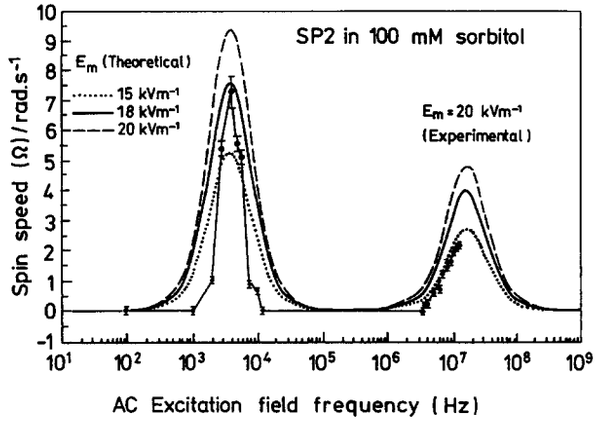

Fig. 10. A fitting between the experimental and theoretical spin speeds for SP2 cells for the various values of the external electric field strengths (i.e. 15, 18 and 20 kV m^{-1}). The following parameters were used for these theoretical plots: $\varepsilon_s = 80\varepsilon_o$, $\varepsilon_c = 60\varepsilon_o$, $\varepsilon_m = 11.1\varepsilon_o$, $\sigma_s = 1$ mS m^{-1}, $\sigma_c = 0.3$ S m^{-1}, $\sigma_m = 10^{-7}$ S m^{-1}, R = 10 μm, $\delta = 10$ nm, $\eta = 1.05$ mN s m^{-2}, $\theta = +23°$.

(2) Microscopically, the membranes of the cells are not smooth at the molecular level. As a result the Navier–Stokes law is not strictly applicable and the effective viscous drag associated with a hydrodynamic effect between the two cells is higher than that expected for a perfect spherical smooth surface. Note that the hydrodynamic interference would not alter the spin resonant frequency; it would merely reduce the rate of spinning.

(3) An error in determining the local electric field; the cell has a finite cell size whilst the field used was that calculated for the centre of the cell. The field variation within a cell is greater for a big cell than a smaller cell. This could result in a significant error in determining the average field used in the calculations.

With a known conductivity of the external medium (σ_s) and by determining the spin resonant frequency (SRF) of each cell , it was found that the specific membrane capacitance for K562 and SP2 were 2.7 ± 0.8 mF m^{-2} and 9.8 ± 0.6 mF m^{-2}, respectively. These estimated values are comparable with the values obtained from the measurements of the dielectrophoretic force on these cell lines by Mahaworasilpa et al. [8], from the cell rotation measurements (for SP2 cells) by Sukhorukov et al. [4]. Table 2 gives a summary of the membrane capacitances of K562

Table 2
A summary of the estimated membrane capacitances for K562 and SP2 cells from the dielectrophoretic force and cell rotation measurements

	Estimated membrane capacitance (mF m^{-2})		
	dielectrophoresis	cell rotation	
	after Mahaworasilpa et al. [8]	present study	after Sukhorukov et al. [4]
K562	2.0 ± 1.0	2.7 ± 0.8	–
SP2	6.0 ± 2.0	9.8 ± 0.6	$\sim 8.1 \pm 0.2$

Note that both cell types were suspended in 100 mM sorbitol.

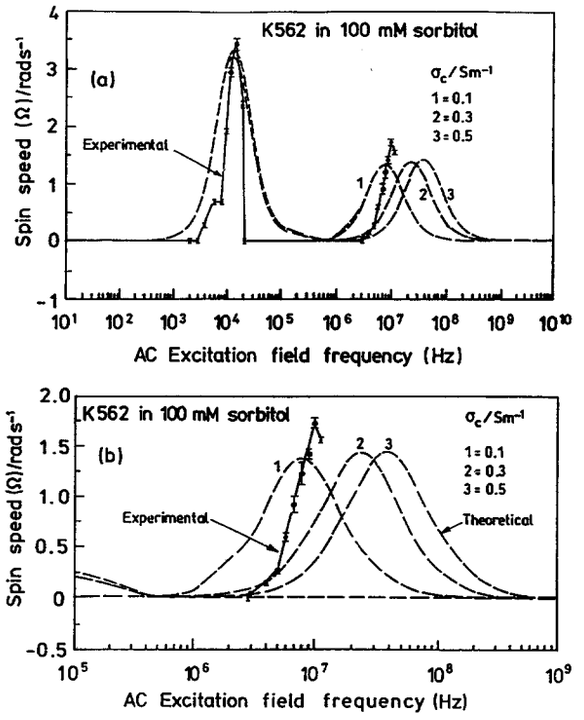

Fig. 11. (a) A spectral fitting between the experimental and theoretical spin speeds for K562 cells for the various theoretical values of σ_c. The parameters used for these theoretical plots were the same as those used in Fig. 9. (b) Enlargement of the high-frequency portion of (a).

and SP2 cells determined from dielectrophoretic measurements [8] and the present electro-rotation study. The value of 9.8 mF m^{-2} for the specific membrane capacitance of SP2 cells is typical for capacitances of biological cells measured by other techniques (e.g. [15,17–20]). The value of 2.7 mF m^{-2} for K562 cells is lower than expected. A lower value by a factor of 3 in the membrane capacitance either indicates that these cells have a dramatically thicker membrane or have a much reduced value for the average dielectric constant of the membrane material. This clearly warrants further investigation.

The conductivity of the intracellular fluid (cytoplasm) has theoretically little effect on the cell spin characteristics in the low-frequency excitation region. However, it has a strong effect on the high-frequency excitation field peak. This is shown in Figs. 11 and 12, where once again, a comparison is made of the experimental cell spin data and theoretical fits for K562 and SP2 cells, respectively. From these fits the conductivity, σ_c, of the cell cytoplasm for K562 and SP2 cells could be estimated from the high-frequency excitation field region (as shown in Fig. 11b and Fig. 12b). Although, the peak value of the spin speed of rotation of each cell type could not be determined experimentally due to the limitations of the function generator, the form of the experimental data leading up to the peak in the high excitation frequency region was used to match, as closely as possible, the theoretical curve using σ_c as an adjustable parameter. It was found that σ_c's for K562 and

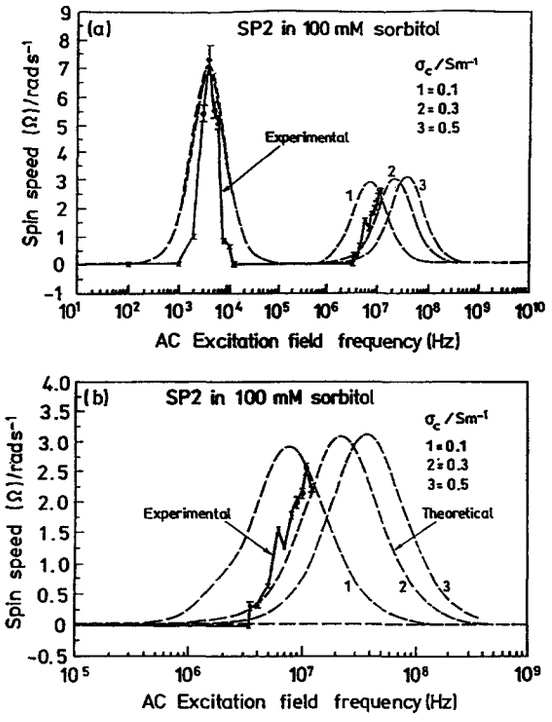

Fig. 12. (a) A spectral fitting between the experimental and the theoretical spin speeds for SP2 cells for the various theoretical values of σ_c. The parameters used for these theoretical plots were the same as those used in Fig. 10. (b) Enlargement of the high-frequency portion of (a).

SP2 cells were estimated to be approximately 0.2 and 0.3 S m^{-1}, respectively, when they were suspended in 100 mM sorbitol solution (with the conductivity σ_s of 1 mS m^{-1}). These estimated values of σ_c are comparable to the value estimated by many investigators by other techniques (e.g. σ_c varies from 0.3 to 0.7 S m^{-1} [18,21]). Table 3 gives a summary of the conductivities of the cell cytoplasms of K562 and SP2 cells from the dielectrophoretic measurements reported by Mahaworasilpa et al. [8] and the present cell electro-rotation measurements.

Acknowledgements

The authors wish to acknowledge the support of the Australian Research Council and the UNESCO Centre for Membrane Science and Technology. Also the authors would like to thank Ms. Cathy Faust and Mr. Chris Pennay for the preparation of all the diagrams presented in this paper.

Appendix A. Torques on biological cells

In the present analysis, we employed a spherical dielectric shell model for biological cells. Consider two identical

Table 3
A summary of the estimated conductivities of the cytoplasms for K562 and SP2 cells from the dielectrophoretic force and cell rotation measurements

	Estimated cytoplasmic conductivity (S m^{-1})	
	dielectrophoresis [8]	cell rotation (present study)
K562	0.15 ± 0.05	0.2
SP2	0.20 ± 0.05	0.3

Note that both cell types were suspended in 100 mM sorbitol.

cells of radius R, with their centres separated by distance r at A and B, in an external, *uniform* alternating electric field $\mathbf{E}_o$ (i.e. for the case when $E_m = E'_m$ = constant) as shown in Fig. 13. Let the cells be arranged such that the axis (**r**) joining between their centres from B to A makes an angle θ with respect to $\mathbf{E}_o$ and let the frequency of the external electric field be in the intermediate frequency domain (e.g. 100 kHz to 3 MHz). In this uniform field, identical *primary* electric dipoles, $\boldsymbol{\mu}_A$ and $\boldsymbol{\mu}_B$ are induced in cell A and cell B, respectively, with their orientations *unparallel* to $\mathbf{E}_o$ due to cell-to-cell interaction (Fig. 13) but in a similar direction as $\mathbf{E}_o$ [8].

Let $\mathbf{E}_{AB}$ and $\mathbf{E}_{BA}$ be the field at A produced by cell B and the field at B produced by cell A, respectively, then the fields at the centres of cell A and cell B will be $\mathbf{E}_A = \mathbf{E}_o + \mathbf{E}_{AB}$ and $\mathbf{E}_B = \mathbf{E}_o + \mathbf{E}_{BA}$ and the induced dipole moments at the centres of cell A and cell B will, respectively, be

$$\boldsymbol{\mu}_A = 4\pi\varepsilon_s R^3 f(\omega)\mathbf{E}_A \quad \text{(A-1)}$$

and

$$\boldsymbol{\mu}_B = 4\pi\varepsilon_s R^3 f(\omega)\mathbf{E}_B \quad \text{(A-2)}$$

where ε_s is the permittivity of external medium; $f(\omega)$ is a complex and complicated function given elsewhere [8].

In Fig. 14 we resolve the induced dipoles $\boldsymbol{\mu}_A$, $\boldsymbol{\mu}_B$ in two components; the **x** and **z** directions. It can be shown that the induced electric fields of a dipole $\boldsymbol{\mu}$ along the unit vector $\hat{r}$ and the unit vector $\hat{\theta}$ are $\mathbf{E}_r =$

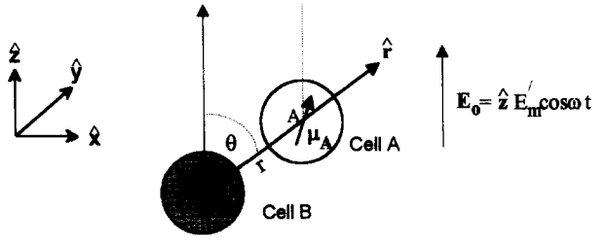

Fig. 13. A diagram showing two identical cells of radius R, with their centres (at A and B) separated by distance r, in an external, uniform electric field $\mathbf{E}_o$.

$(2\mu\cos\theta/4\pi\varepsilon_s r^3)\hat{r}$ and $\mathbf{E}_\theta = (\mu\sin\theta/4\pi\varepsilon_s r^3)\hat{\theta}$, respectively, where θ is the angle made between $\mathbf{E}_o$ and $\mathbf{r}$ in the *clockwise* direction. From Fig. 14, we can deduce the induced electric fields $(E_A)_x$ and $(E_A)_z$ due to $(\mu_B)_x$ and $(\mu_B)_z$, and $(E_B)_x$ and $(E_B)_z$ due to $(\mu_A)_x$ and $(\mu_A)_z$ as:

$$(E_A)_x = \frac{3(\mu_B)_z \sin\theta\cos\theta}{4\pi\varepsilon_s r^3} + \frac{(\mu_B)_x(3\sin^2\theta - 1)}{4\pi\varepsilon_s r^3} \tag{A-3}$$

$$(E_A)_z = E_o + \frac{(\mu_B)_z(3\cos^2\theta - 1)}{4\pi\varepsilon_s r^3} + \frac{3(\mu_B)_x \sin\theta\cos\theta}{4\pi\varepsilon_s r^3} \tag{A-4}$$

$$(E_B)_x = \frac{3(\mu_A)_z \sin\theta\cos\theta}{4\pi\varepsilon_s r^3} + \frac{(\mu_A)_x(3\sin^2\theta - 1)}{4\pi\varepsilon_s r^3} \tag{A-5}$$

$$(E_B)_z = E_o + \frac{(\mu_A)_z(3\cos^2\theta - 1)}{4\pi\varepsilon_s r^3} + \frac{3(\mu_A)_x \sin\theta\cos\theta}{4\pi\varepsilon_s r^3} \tag{A-6}$$

Substituting $(\mu_A)_x$, $(\mu_A)_z$, $(\mu_B)_x$ and $(\mu_B)_z$ from Eq. A-1 and Eq. A-2 into Eq. A-3 to Eq. A-6 gives

$$(E_A)_x = 3(R/r)^3 f(\omega)(E_B)_z \sin\theta\cos\theta + (R/r)^3 f(\omega)(E_B)_x(3\sin^2\theta - 1) \tag{A-7}$$

$$(E_A)_z = E_o + (R/r)^3 f(\omega)(E_B)_z(3\cos^2\theta - 1) + 3(R/r)^3 f(\omega)(E_B)_x \sin\theta\cos\theta \tag{A-8}$$

$$(E_B)_x = 3(R/r)^3 f(\omega)(E_A)_z \sin\theta\cos\theta + (R/r)^3 f(\omega)(E_A)_x(3\sin^2\theta - 1) \tag{A-9}$$

$$(E_B)_z = E_o + (R/r)^3 f(\omega)(E_A)_z(3\cos^2\theta - 1) + 3(R/r)^3 f(\omega)(E_A)_x \sin\theta\cos\theta \tag{A-10}$$

Substituting $(E_B)_x$ and $(E_B)_z$ from Eq. A-9 and Eq. A-10 into Eq. A-7 and Eq. A-8 gives

$$(E_A)_x = hE_o + c(E_A)_z + p(E_A)_x \tag{A-11}$$

$$(E_A)_y = aE_o + b(E_A)_z + c(E_A)_x \tag{A-12}$$

where

$$a = 1 + (R/r)^3 f(\omega)(3\cos^2\theta - 1) \tag{A-13}$$

$$b = (R/r)^6 f^2(\omega)(3\cos^2\theta + 1) \tag{A-14}$$

$$c = 3(R/r)^6 f^2(\omega)\sin\theta\cos\theta \tag{A-15}$$

$$h = 3(R/r)^3 f(\omega)\sin\theta\cos\theta \tag{A-16}$$

$$p = (R/r)^6 f^2(\omega)(3\sin^2\theta + 1) \tag{A-17}$$

The solutions of Eq. A-11 and Eq. A-12 are

$$(E_A)_x = E_o\left(\frac{(1-b)h + ac}{(1-b)(1-p) - c^2}\right) \tag{A-18}$$

$$(E_A)_z = E_o\left(\frac{a(1-p) + ch}{(1-b)(1-p) - c^2}\right) \tag{A-19}$$

Substituting Eq. A-18 and Eq. A-19 into Eq. A-9 and Eq. A-10, it follows that $(E_B)_x = (E_A)_x$ and $(E_B)_z = (E_A)_z$. Substituting Eq. A-13 to Eq. A-17 into Eq. A-18 and Eq. A-19, we can then simplify $(E_A)_x$ and $(E_A)_z$ as:

$$(E_A)_x = \frac{3}{2}E_o \sin 2\theta \times\left(\frac{(R/r)^3 f(\omega)}{1 - (R/r)^3 f(\omega) - 2(R/r)^6 f^2(\omega)}\right) = \frac{3}{2}E_o \sin 2\theta \cdot g_x(\omega) \tag{A-20}$$

$$(E_A)_z = \frac{1}{2}E_o\left(\frac{2 - (R/r)^3 f(\omega)(1 - 3\cos 2\theta)}{1 - (R/r)^3 f(\omega) - 2(R/r)^6 f^2(\omega)}\right) = \frac{1}{2}E_o\, g_z(\omega,\theta) \tag{A-21}$$

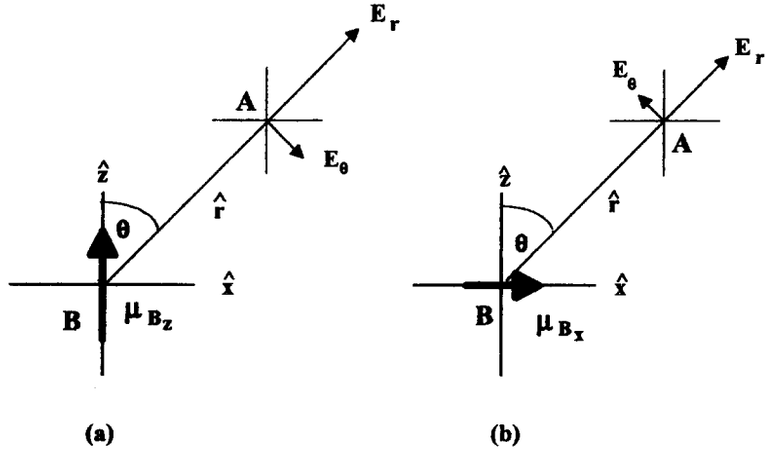

(a) (b)

Fig. 14. Diagrams showing the induced electric fields $\mathbf{E}_r$ and $\mathbf{E}_\theta$ at the centre of cell A (point A) due to each component of the electric dipole μ_B (i.e. the x and z components) induced in cell B.

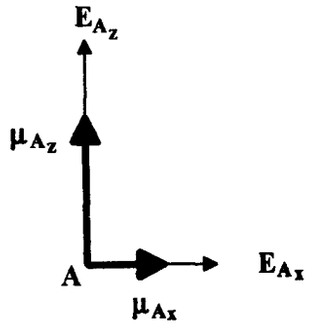

Fig. 15. A spatial diagram for μ_A's and E_A's in the x and z axes.

It can be seen from Eq. A-20 and Eq. A-21 that $(E_A)_x$ and $(E_A)_z$ are out of phase with E_o by angles ϕ_1 and ϕ_2 due to the complex nature of the functions $g_x(\omega)$ and $g_z(\omega,\theta)$, respectively. That is

$$\phi_1 = \tan^{-1}\frac{\mathrm{Im}[g_x(\omega)]}{\mathrm{Re}[g_x(\omega)]} \quad \text{and}$$

$$\phi_2 = \tan^{-1}\frac{\mathrm{Im}[g_z(\omega,\theta)]}{\mathrm{Re}[g_z(\omega,\theta)]}$$

where Im and Re denote the imaginary and the real part of $g(\omega)$, respectively. From Eq. A-1, we can write $(\mu_A)_x$ and $(\mu_A)_z$ as:

$$(\mu_A)_x = 4\pi\varepsilon_s R^3 f(\omega)(E_A)_x \tag{A-22}$$

$$(\mu_A)_z = 4\pi\varepsilon_s R^3 f(\omega)(E_A)_z \tag{A-23}$$

Eq. A-22 and Eq. A-23 indicate that both $(\mu_A)_x$ and $(\mu_A)_z$ are out of phase by γ with $(E_A)_x$ and $(E_A)_z$, respectively. The phase difference γ is obtained from $\gamma = \tan^{-1}(\mathrm{Im}[f(\omega)]/\mathrm{Re}[f(\omega)])$. It follows from the above that $(\mu_A)_x$ is out of phase with E_o by $\gamma + \phi_1$, whereas $(\mu_A)_z$ is out of phase with E_o by $\gamma + \phi_2$. Fig. 15 shows a spatial diagram for μ_A's and E_A's. The interaction between μ_A's and E_A's produces a total rotating torque τ_t which can be given by

$$\tau_t = \tau_1 + \tau_2 = (\mu_A)_z \times (\mathbf{E}_A)_x + (\mu_A)_x \times (\mathbf{E}_A)_z \tag{A-24}$$

The time-average of the total torque is then given by

$$\overline{\tau_t} = \overline{(\mu_A)_z (E_A)_x - (\mu_A)_x (E_A)_z} \tag{A-25}$$

Note that we assign the *positive* sign for the *clockwise* torque, whereas the *negative* sign for the *anti-clockwise* torque.

From Eq. A-20 and Eq. A-23, we can write

$$(E_A)_x = \frac{3}{2}E'_m \sin 2\theta\, |g_x(\omega)| \cos(\omega t + \phi_1) \tag{A-26}$$

and

$$(\mu_A)_z = 2\pi\varepsilon_s R^3 E'_m\, |f(\omega)\cdot g_z(\omega,\theta)| \cos(\omega t + \gamma + \phi_2) \tag{A-27}$$

where $|f(\omega)|$, $|g_z(\omega,\theta)|$ and $|g_x(\omega)|$ are the moduli of $f(\omega)$, $g_z(\omega,\theta)$ and $g_x(\omega)$, respectively. Therefore the time-average of the first expression on the right hand side of Eq. A-25 can be written as

$$\begin{aligned}
&\overline{(\mu_A)_z (E_A)_x} \\
&= \lambda |f(\omega)\cdot g_z(\omega,\theta)| \cdot |g_x(\omega)| \\
&\quad \overline{\cos(\omega t + \gamma + \phi_2)\cos(\omega t + \phi_1)} \\
&= \frac{\lambda}{2} |f(\omega)\cdot g_z(\omega,\theta)| \cdot |g_x(\omega)| \\
&\quad \times \{\cos(\gamma + \phi_2)\cos\phi_1 + \sin(\gamma + \phi_2)\sin\phi_1\} \\
&= \frac{\lambda}{2}\{\mathrm{Re}[f(\omega)\cdot g_z(\omega,\theta)]\,\mathrm{Re}[g_x(\omega)] \\
&\quad + \mathrm{Im}[f(\omega)\cdot g_z(\omega,\theta)]\,\mathrm{Im}[g_x(\omega)]\}
\end{aligned} \tag{A-28}$$

where

$$\lambda = 3\pi\varepsilon_s R^3 E'^2_m \sin 2\theta \tag{A-28a}$$

Similarly,

$$\begin{aligned}
&\overline{(\mu_A)_x (E_A)_z} \\
&= \frac{\lambda}{2}\{\mathrm{Re}[f(\omega)\cdot g_x(\omega)]\,\mathrm{Re}[g_z(\omega,\theta)] \\
&\quad + \mathrm{Im}[f(\omega)\cdot g_x(\omega)]\,\mathrm{Im}[g_z(\omega,\theta)]\}
\end{aligned} \tag{A-29}$$

Substituting Eq. A-28 and Eq. A-29 into Eq. A-25 gives

$$\begin{aligned}
\overline{\tau_t} = \frac{\lambda}{2}\{&(\mathrm{Re}[f(\omega)\cdot g_z(\omega,\theta)]\,\mathrm{Re}[g_x(\omega)] \\
&+ \mathrm{Im}[f(\omega)\cdot g_z(\omega,\theta)]\,\mathrm{Im}[g_x(\omega)]) \\
&-(\mathrm{Re}[f(\omega)\cdot g_x(\omega)]\,\mathrm{Re}[g_z(\omega,\theta)] \\
&+ \mathrm{Im}[f(\omega)\cdot g_x(\omega)]\,\mathrm{Im}[g_z(\omega,\theta)])\}
\end{aligned} \tag{A-30}$$

or

$$\begin{aligned}
\overline{\tau_t} = \frac{\lambda}{2}\mathrm{Re}\{&[f(\omega)\cdot g_z(\omega,\theta)]\cdot[g_x^*(\omega)] \\
&-[f(\omega)\cdot g_x(\omega)]\cdot[g_z^*(\omega,\theta)]\}
\end{aligned} \tag{A-31}$$

where $g_x^*(\omega)$ and $g_z^*(\omega,\theta)$ are the complex conjugates of $g_x(\omega)$ and $g_z(\omega,\theta)$, respectively, and $[f(\omega)\cdot g(\omega)]$ is the complex quantity of the product of $f(\omega)$ and $g(\omega)$.

When cell A and cell B are in contact, $(R/r)^3 = 1/8$. Since $-0.5 < f(\omega) < 1$, $(R/r)^6 f^2(\omega)$ can be considered small and negligible. Therefore, $g_x(\omega)$ and $g_z(\omega,\theta)$ from Eq. A-20 and Eq. A-21 can be simplified to

$$g_x(\omega) = \frac{f(\omega)}{8 - f(\omega)} \quad \text{and} \quad g_z(\omega,\theta) = \frac{16 - \chi\cdot f(\omega)}{8 - f(\omega)}$$

(where $\chi = 1 - 3\cos 2\theta$).

Their complex conjugates can be deduced as

$$g_x^*(\omega) = \frac{f^*(\omega)}{8 - f^*(\omega)} \quad \text{and} \quad g_z^*(\omega,\theta) = \frac{16 - \chi \cdot f^*(\omega)}{8 - f^*(\omega)}$$

Substituting g_x, g_z and their conjugates into Eq. A-31 gives

$$\overline{\tau}_t = \frac{\lambda}{2} \mathrm{Re}\left(\frac{f(\omega) f^*(\omega)[16 - \chi \cdot f(\omega)]}{[8 - f(\omega)][8 - f^*(\omega)]} - \frac{f^2(\omega)[16 - \chi \cdot f^*(\omega)]}{[8 - f(\omega)][8 - f^*(\omega)]} \right) = \frac{\lambda}{2} \mathrm{Re}\left(\frac{16[f(\omega) \cdot f^*(\omega) - f^2(\omega)]}{64 - 8[f(\omega) + f^*(\omega)] + f(\omega) \cdot f^*(\omega)} \right) \quad \text{(A-32)}$$

The function $f(\omega)$ and its conjugate can be written as $f(\omega) = \mathrm{Re}[f(\omega)] + j\mathrm{Im}[f(\omega)]$ and $f^* = \mathrm{Re}[f(\omega)] - j\mathrm{Im}[f(\omega)]$. Therefore, Eq. A-32 can be simplified to

$$\overline{\tau}_t = \frac{\lambda}{2} \mathrm{Re}\left(\frac{32\{\mathrm{Im}^2[f(\omega)] - j\mathrm{Re}[f(\omega)]\,\mathrm{Im}[f(\omega)]\}}{64 - 16\mathrm{Re}[f(\omega)] + |f(\omega)|^2} \right) \quad \text{(A-33)}$$

$|f(\omega)|^2$ in the denominator of Eq. A-33 can be neglected since $|f(\omega)|^2 < 64$. Then Eq. A-33 can be simplified to

$$\overline{\tau}_t = \lambda \left(\frac{\mathrm{Im}^2[f(\omega)]}{4 - \mathrm{Re}[f(\omega)]} \right) \quad \text{(A-34)}$$

where λ is given previously (see Eq. A-28a),

$$\mathrm{Re}[f(\omega)] = -\left[\frac{AB + CD\omega^2}{B^2 + D^2\omega^2} \right] \quad \text{(A-35)}$$

$$\mathrm{Im}[f(\omega)] = -\omega\left[\frac{BC - AD}{B^2 + D^2\omega^2} \right] \quad \text{(A-36)}$$

and A, B, C and D are given by Mahaworasilpa et al. [8].

References

[1] Huang, Y., Holzel, R., Pethig, R. and Wang, X.-B. (1992) Phys. Med. Biol. 37, 1499–1517.
[2] Fuhr, G., Geissler, F., Muller, T., Hagedorn, R. and Torner, H. (1987) Biochim. Biophys. Acta 930, 65–71.
[3] Hu, X., Arnold, W.M. and Zimmermann, U. (1990) Biochim. Biophys. Acta 1021, 191–200.
[4] Sukhorukov, V.L., Arnold, W.M. and Zimmermann, U. (1993) J. Membr. Biol. 132, 27–40.
[5] Wang, X.-B., Huang, Y., Gascoyne, P.R.C., Becker. F.F., Holzel, R. and Pethig, R. (1994) Biochim. Biophys. Acta 1193, 330–344.
[6] Furedi, A.A. and Valentine, R.C. (1962) Biochim. Biophys. Acta 56, 33–42.
[7] Pohl, H.A. (1978) in Dielectrophoresis, Cambridge University Press, London.
[8] Mahaworasilpa, T.L., Coster, H.G.L. and George, E.P. (1994) Biochim. Biophys. Acta 1193, 118–126.
[9] Arnold, W.M. and Zimmermann, U. (1982) Z. Naturforsch. 37c, 908–915.
[10] Fuhr, G. and Kuzmin, P.I. (1986) Biophys. J. 50, 789–795.
[11] Teixeira-Pinto, A.A., Nejelski, L.L. Cutler, J.L. and Heller, J.H. (1960) Exp. Cell Res. 20, 548–564.
[12] Holzapfel, C., Vienken, J. and Zimmermann, U. (1982) J. Membr. Biol. 67, 13–26.
[13] Mischel, M. and Pohl, H.A. (1983) J. Biol. Phys. 11, 98–102.
[14] Pohl, H.A. (1983) J. Biol. Phys. 11, 59–62.
[15] Arnold, W.M., Schmutzler, R.K., Schmutzler, A.G., Van der Ven, H., Al-Hasani, S., Krebs, D. and Zimmermann, U. (1987) Biochim. Biophys. Acta 905, 454–464.
[16] Gimsa, J., Marszalek, P., Loewe, U. and Tsong, T.Y. (1991) Biophys. J. 60, 749–760.
[17] Coster, H.G.L. and Smith, J.R. (1974) Biochim. Biophys. Acta 373, 151–164.
[18] Fricke, H. and Morse, S. (1925) J. Gen. Physiol. 9, 153–167.
[19] Fricke, H. and Curtis, H.J. (1935) Nature 135, 436.
[20] Kaler, K.V.I.S. and Jones, T.B. (1990) Biophys. J. 57, 173–182.
[21] Pauly, H. and Schwan, H.P. (1966) Z. Naturforsch. 14b, 125–131.
[22] Lamb, H. (1906) Hydrodynamics, 3rd Edn., Article 322, Cambridge University, Cambridge, UK.
[23] Zimmermann, U., Vienken, J. and Pilwat, G. (1981) Z. Naturforsch. 36c, 173–177.
[24] Sauer, F.A. and Schlogl, R.W. (1985) in Interactions between Electromagnetic Fields and Cells (Chiabrere, A., Nicolini, C. and Schwan, H.P., eds.), pp. 203–251, Plenum Press, New York.